Determination of Pore Size and Pore Wall Structure of MCM-41 by Using Nitrogen Adsorption, Transmission Electron Microscopy, and X-ray Diffraction

Michal Kruk and Mietek Jaroniec*

Department of Chemistry, Kent State University, Kent, Ohio 44240

Yasuhiro Sakamoto[†] and Osamu Terasaki[†,‡]

Department of Physics, Graduate School of Science and Center of Interdisciplinary Research, Tohoku University, Sendai, 980-77, Japan, and CREST, Japan Science and Technology Corporation, Japan

Ryong Ryoo and Chang Hyun Ko

Department of Chemistry and Center for Molecular Science, Korea Advanced Institute of Science and Technology, Taeduk Science Town, Taejon, 305−701 Korea

Received: August 2, 1999; In Final Form: November 3, 1999

Highly ordered MCM-41 materials were synthesized using single or mixed alkyltrimethylammonium and alkyltriethylammonium surfactants of alkyl chain lengths from 12 to 22. As determined using combined adsorption/powder X-ray diffraction (XRD) analysis, the obtained samples exhibited pore sizes from 3.2 to 4.8 nm with about 0.3 nm increments. Nitrogen adsorption isotherms for the samples under study exhibited remarkably sharp capillary condensation steps. The adsorption isotherm for the highly ordered 4.8 nm MCM-41 featured a narrow hysteresis loop with parallel adsorption and desorption branches. This behavior is probably a feature of nitrogen adsorption in ideal cylindrical pores of this size and is distinctly different from the previously reported behavior of MCM-41 with pore sizes in the range 4−5.5 nm, which had triangular hysteresis loops on their nitrogen adsorption isotherms. All MCM-41 materials had remarkably narrow pore size distributions, which showed that fine-tuning of the pore size is easily achievable for the synthesis procedure used. The pore wall thickness was found to increase as the pore size increased. The pore wall thickness determined using transmission electron microscopy (TEM) was somewhat larger than that obtained using the combined XRD/adsorption analysis, which was attributed to inherent features of these determination methods. TEM images showed that pores of MCM-41 samples were approximately hexagonal rather than circular, thus providing structural information especially important for application of MCM-41 as a model adsorbent. Low-pressure adsorption studies of uncalcined ethanol-washed MCM-41 samples revealed that external surfaces of their particles were covered by relatively dense layers of surfactant ions. This behavior is consistent with the generally accepted mechanism of the MCM-41 formation via self-assembly of silicate−surfactant ion pairs. Comparison of adsorption isotherms for uncalcined and calcined samples allowed us to exclude the possibility of any appreciable structural degradation during calcination, although TEM provided some indication of the lowering of structural ordering upon calcination.

1. Introduction

Recently, we have witnessed the discovery of ordered mesoporous materials (OMMs)[1,2] and an explosive growth of research in this area.[3−10] Despite many remarkable achievements in the synthesis and application of OMMs,[3−11] their structures and mechanisms of formation are still the subject of a vigorous debate.[3−12] One of the crucial problems is determination of their pore shape, pore diameter, and pore wall thickness.[5,8,12,13] Recently, a method for determination of the pore size of MCM-41, the most commonly studied and applied OMM, has been proposed[14,15] on the basis of the geometrical relation between the interplanar spacing, pore volume, and pore diameter for the honeycomb structure. Since the interplanar spacing and volume of ordered mesopores are usually obtained from a routine XRD and adsorption characterization of MCM-41, the aforementioned geometrical approach can easily be applied. Moreover, this method was shown to be consistent with nitrogen adsorption data[15−18] and was suggested to be suitable for accurate pore wall thickness determination.[15,16] The derivation of the geometrical relations for the pore size and pore wall thickness evaluation rests upon the assumption about the particular pore geometry but the differences in results for two most commonly accepted MCM-41 pore geometries (that is, circular and hexagonal) are relatively small.[12]

To our best knowledge, the accuracy and the underlying assumptions of the geometrical method have never been questioned in the literature, thus making it a candidate for a standard method for evaluation of the pore size and pore wall thickness of MCM-41 materials. On the basis of the pore size estimates from the geometrical method, it was demonstrated

* Corresponding author: Phone: (330) 672 3790. Fax: (330) 672 3816. E-mail: jaroniec@columbo.kent.edu.
[†] Tohoku University.
[‡] Japan Science and Technology Corporation.

10.1021/jp992718a CCC: $19.00
Published on Web 12/09/1999

that adsorption rather than desorption branches of nitrogen isotherms are suitable for the pore size analysis.[17] Moreover, application of a proper calibration procedure developed by Kruk, Jaroniec, and Sayari (KJS) allowed us to establish an unambiguous and simple relation between the capillary condensation pressure and the diameter of siliceous cylindrical pores.[17] This relation can conveniently be employed in various methods of the mesopore size determination,[19,20] thus providing the long awaited general, simple, and accurate method for the mesopore size analysis. The KJS approach was also extended to mesoporous materials with strongly hydrophobic surfaces.[21]

It is important to further verify the underlying assumptions of the geometrical method for the pore diameter and pore wall thickness evaluation and compare the results of this approach with some other well-established characterization techniques. In particular, high-resolution transmission electron microscopy (HRTEM) is a good candidate for such a comparison, since it is a powerful and highly informative method for elucidation of structure of OMMs, allowing determination of the pore structure symmetry, pore shape, pore wall thickness, and so forth.[13,22−28] From the previously reported results, one can conclude that the pore wall thickness of MCM-41 determined on the basis of the geometrical considerations using adsorption/XRD data (which usually lies between 0.6 and 1.3 nm) was in good agreement with pore wall thicknesses evaluated using TEM[22] and simulation of XRD spectra.[29−31] In contrast, the results obtained from more routine TEM or adsorption/XRD studies often indicated much larger pore wall thicknesses. This can primarily be attributed to the fact that HRTEM requires proper methods of data analysis in order to avoid artifacts, which lead for instance to determination of an overestimated pore wall thickness[13] or incorrect pore shape.[27,28] Likewise, adsorption methods for the mesopore size evaluation are often based on application of the grossly inaccurate Kelvin equation, inaccurate statistical film thickness curves, and so forth,[17] which lead to the pore size underestimation and the pore wall thickness overestimation.

The aim of the current study was to thoroughly characterize a series of highly ordered MCM-41 silicas with a wide range of pore sizes using XRD, HRTEM, and nitrogen adsorption in order to gain new insight into their structures and to confirm some previously reported features of MCM-41.

2. Materials and Methods

2.1. Materials. The MCM-41 samples under study were synthesized using alkyltrimethylammonium ($C_nH_{2n+1}(CH_3)_3N^+$; $n = 12$, 14), alkyltriethylammonium ($C_nH_{2n+1}(C_2H_5)_3N^+$; $n = 22$), or mixtures of alkyltrimethylammonium and alkyltriethylammonium surfactants of the same alkyl chain length ($n = 16$, 18, and 20) as structure directing agents. The surfactant mixing ratio was optimized according to the length of the C_n alkyl groups, to achieve a micelle packing suitable for formation of a given hexagonal mesophase. The synthesis of the MCM-41 silica was performed in a manner similar to that reported in our previous works,[32,33] as described in detail elsewhere.[34] In brief, an aqueous solution of sodium silicate with Na/Si = 0.5 (2.4 wt % Na_2O, 9.2 wt % SiO_2, 88.4 wt % H_2O) and an aqueous solutions of surfactant were prepared at various temperatures depending on C_n as given in Table 1. The silica source was added drop by drop to the surfactant solutions with vigorous stirring at the same temperatures. After continuously stirred for 1 h, the resultant gel mixtures were heated for 24 h at 373 K. The mixtures after heating were cooled to the same temperatures as before the initial mixing, and pH of the mixture was adjusted to 10 with acetic acid. The mixtures after the pH adjustment were heated again for 2 d at 373 K. The pH adjustment and subsequent heating were repeated once more before precipitated MCM-41 products were finally filtered. After synthesis, the MCM-41 samples containing surfactant were washed by slurrying for 10 min in an ethanol/HCl mixture (1 g of as-synthesized MCM-41 with a mixture of 0.5 mL of 37% HCl plus 20 mL of 95% ethanol). The washed samples were immediately dried in an oven at 393 K. More than 95% of the surfactant was removed from the MCM-41 samples by this washing treatment. These ethanol/acid washed samples are denoted Cn-EA MCM-41. Cn-EA MCM-41 samples were calcined in air at 823 K, and the resulting samples are denoted Cn MCM-41. Alternatively, after the synthesis, the samples containing surfactant were washed with ethanol only. These materials are denoted Cn-E MCM-41.

TABLE 1: Optimum Conditions for MCM-41 Synthesis[a]

samples	molar composition of starting mixtures $C_nH_{2n+1}N(CH_3)_3Br$	$C_nH_{2n+1}N(C_2H_5)_3Br$	H_2O	mixing temp (K)
C22	0	1	500	338
C20	0.10	0.90	500	333
C18	0.66	0.34	400	328
C16	0.80	0.20	400	303
C14	1	0	400	293
C12	1	0	400	293

[a] The composition of the starting mixtures was $4SiO_2/1Na_2O/xC_n$ TMABr/yC_n TEABr/zH_2O, where the mole numbers x, y, and z are given in the table.

2.2. Measurements. XRD measurements were performed on a Rigaku Miniflex (0.5 kW) instrument using Cu−Kα radiation with 0.01° 2θ step size and 1 s step time. For TEM measurements, all MCM-41 materials were crushed in an agate mortar, dispersed in ethanol, and deposited on a microgrid. A TEM model JEM-3010 (side-entry goniometer, Cs = 0.6 mm, accelerating voltage = 300 kV) was used. HRTEM images were recorded by both films and a MultiScan CCD camera (model 794, Gatan, size 1024 × 1024, pixel size 25 × 25 μm) at about 100 000 times magnification using low dose conditions, although the materials were much stronger for the electron beam than zeolites. Nitrogen adsorption measurements were performed at 77 K on an ASAP 2010 volumetric adsorption analyzer manufactured by Micromeritics, Norcross, GA. Before the adsorption analysis, the calcined samples were outgassed for 2 h at 473 K in the degas port of the adsorption analyzer, whereas the uncalcined ethanol-washed samples were outgassed at room temperature to avoid the surfactant decomposition. Weight change curves were acquired using a high-resolution TGA 2950 thermogravimetric analyzer from TA Instruments, New Castle, DE. TGA measurements were performed under nitrogen flow using the maximum heating rate of 5 K/min.

2.3. Characterization Methods. In the TEM analysis, the profiles of image contrast on the lines through the centers of the channels were analyzed by a Digital Micrograph (Gatan) software. The profiles were fitted by Gaussian curves. The threshold to give boundary between the wall and vacuum in the potential density profiles was determined so as to give the correct value for the image simulation for hypothetical mesoporous materials with reasonable density of amorphous silica. It should be noted that all HRTEM images are projected along the incident beam direction, therefore the pore wall thickness value from HRTEM is the projection of the pore walls along this direction and thus is expected to be somewhat higher than the actual pore wall thickness.

The BET specific surface area, S_{BET},[20,35] was calculated using nitrogen adsorption data in the relative adsorption range from

TABLE 2: Structural Properties of the MCM-41 Samples Derived from XRD, TEM, and Nitrogen Adsorption Data

	unit cell parameter (nm)				pore wall thickness (nm)		
	XRD		TEM				
sample	as-synthesized	calcined	calcined	EtOH/HCl washed	EtOH/HCl washed	calcined	eq 1 calcined
C22	5.54	5.64	5.64	5.61	1.80	1.85	1.07
C20	5.23	5.28	5.28	5.26	1.50	1.61	0.98
C18	5.07	4.94	4.84	4.97	1.30	1.56	1.00
C16	4.76	4.61	4.69	4.56	1.18	1.28	0.92
C14	4.32	4.23	4.21	4.25	1.00	1.26	0.89
C12	3.82	3.88	3.80	3.90	0.80	1.10	0.87

0.04 to 0.2, except for C12 MCM-41 for which the interval from 0.04 to 0.1 was used to avoid inclusion of the data points considerably affected by the capillary condensation in primary mesopores of the sample. Note that according to IUPAC recommendations,[35] pores are classified as micropores (width below 2 nm), mesopores (width between 2 and 50 nm), and macropores (width greater than 50 nm). In the current work, ordered mesopores are referred to as primary mesopores. Larger mesopores and small macropores (from about 5 to 200−400 nm) in which capillary condensation takes place at relative pressures higher than those for capillary condensation in primary mesopores and yet distinguishable from the saturation vapor pressure (up to about 0.995) are referred to as secondary mesopores. The total pore volume, V_t, was estimated on the basis of the amount adsorbed at a relative pressure of about 0.99.[20,35] The relative adsorption as a function of relative pressure was obtained by dividing the amount adsorbed by the BET monolayer capacity for a given sample.[16] The primary mesopore volume, V_p, and the external surface area, S_{ex}, were determined using the α_s plot method[16,20] from the adsorption data in the range of the standard reduced adsorption, α_s, from 1.3 to 1.9 (in the case of C12, C14, C20, and C22) or from 1.3 to 1.8 (in the case of C16 and C18). The α_s plot method was also applied to show the lack of microporosity in the calcined materials under study. In this case, the data from the α_s interval from 0.0 to 0.7 were used. The ethanol-washed uncalcined samples were also studied using the α_s plot method, but in this case, the reference adsorption isotherm for highly hydrophobic surfaces was used.[21]

The primary mesopore diameter, w_d, and the pore wall thickness, b_d, were determined using the following equation based on geometrical considerations of the ordered honeycomb structure:[14,15]

$$w_d = cd\left(\frac{\rho V_p}{1+\rho V_p}\right)^{1/2} \qquad (1)$$

where d is the XRD (100) interplanar spacing, c is a constant characteristic of the pore geometry, and ρ is the pore wall density (assumed to be 2.2 cm^3/g for silicas with amorphous pore walls).[14,15] The constant c is equal to 1.213 for circular as well as hexagonal pores, but in the latter case, pore diameter, w_d, is defined as the diameter of a circle of the same area as the hexagonal pore cross section.[12] The pore wall thickness, b_d, was calculated under assumption of the hexagonal pore geometry, as observed from HRTEM. In such a case, b_d is equal to the unit cell parameter, a ($a = 2(3^{-1/2})d$), minus the distance between the midpoints of the sides of the hexagonal cross section (equal to $w_d/1.050$); $b_d = 2(3^{-1/2})d - w_d/1.050$.

The primary mesopore diameter was also evaluated using the BJH method[21] with the corrected form of the Kelvin equation and the statistical film thickness curve for porous silicas, both derived using the KJS approach.[17] The corrected Kelvin equation assumes the form[20]

$$r(p/p_0)\ [nm] = \frac{2\gamma V_L}{RT\ln(p_0/p)} + t(p/p_0) + 0.3 \qquad (2)$$

where p is the equilibrium vapor pressure, p_0 is the saturation vapor pressure, p/p_0 is the relative pressure, $r(p/p_0)$ is the pore radius as a function of the relative pressure, γ and V_L are the surface tension and the molar volume of liquid nitrogen at 77 K, R is the universal gas constant, and T is absolute temperature ($\gamma = 8.88 \times 10^{-3}$ N m^{-1}, $V_L = 34.68$ cm^3 mol^{-1}, and $R = 8.314$ J mol^{-1} K^{-1}). The statistical film thickness (as a function of the relative pressure) for nitrogen adsorbed on the pore walls, $t(p/p_0)$, later referred to as the t curve, was based on the adsorption isotherm for a macroporous silica gel LiChrospher Si-4000.[17] This t curve is essentially the same as the t curve reported later[36] and can be approximated by the following empirical equation valid down to the relative pressure of at least 0.1:[17]

$$t(p/p_0)\ [nm] = 0.1\left[\frac{60.65}{0.03071 - \log(p/p_0)}\right]^{0.3968} \qquad (3)$$

The primary mesopore diameter evaluated on the basis of the KJS approach by employing the BJH algorithm, w_{KJS}, is defined as a maximum on the pore size distribution. The statistical thickness of nitrogen film in the MCM-41 pores was evaluated as described elsewhere.[17]

3. Results and Discussion

3.1. Powder X-ray Diffraction. XRD spectra for the MCM-41 samples under study were reported elsewhere.[34] The values of the XRD unit cell parameters are listed in Table 2. The unit cell parameter for the calcined samples was found to systematically increase by about 0.35 nm for each additional $-(CH_2)_2-$ unit in the alkyl chain of the surfactant (or surfactants) used as templates. This increase is similar to those reported in earlier studies.[15,37] All the XRD patterns exhibited at least four pronounced peaks indicating high structural ordering of the MCM-41 materials. It is interesting to note that the MCM-41 samples prepared using surfactants with eicosyl (C20) and docosyl (C22) alkyl chains were also highly ordered, similarly to the materials prepared using surfactants with shorter alkyl chains. This can be attributed to the application of a surfactant mixture[34,38−41] in the case of C20 MCM-41 and a large headgroup surfactant[34,38] in the case of C22 MCM-41. Otherwise, it is difficult to prepare good quality MCM-41 with long-chain surfactants, for instance with alkyltrimethylammonium,[38] and such a synthesis was so far successful only with docosyltrimethylammonium in weakly basic media (pH = 8).[39]

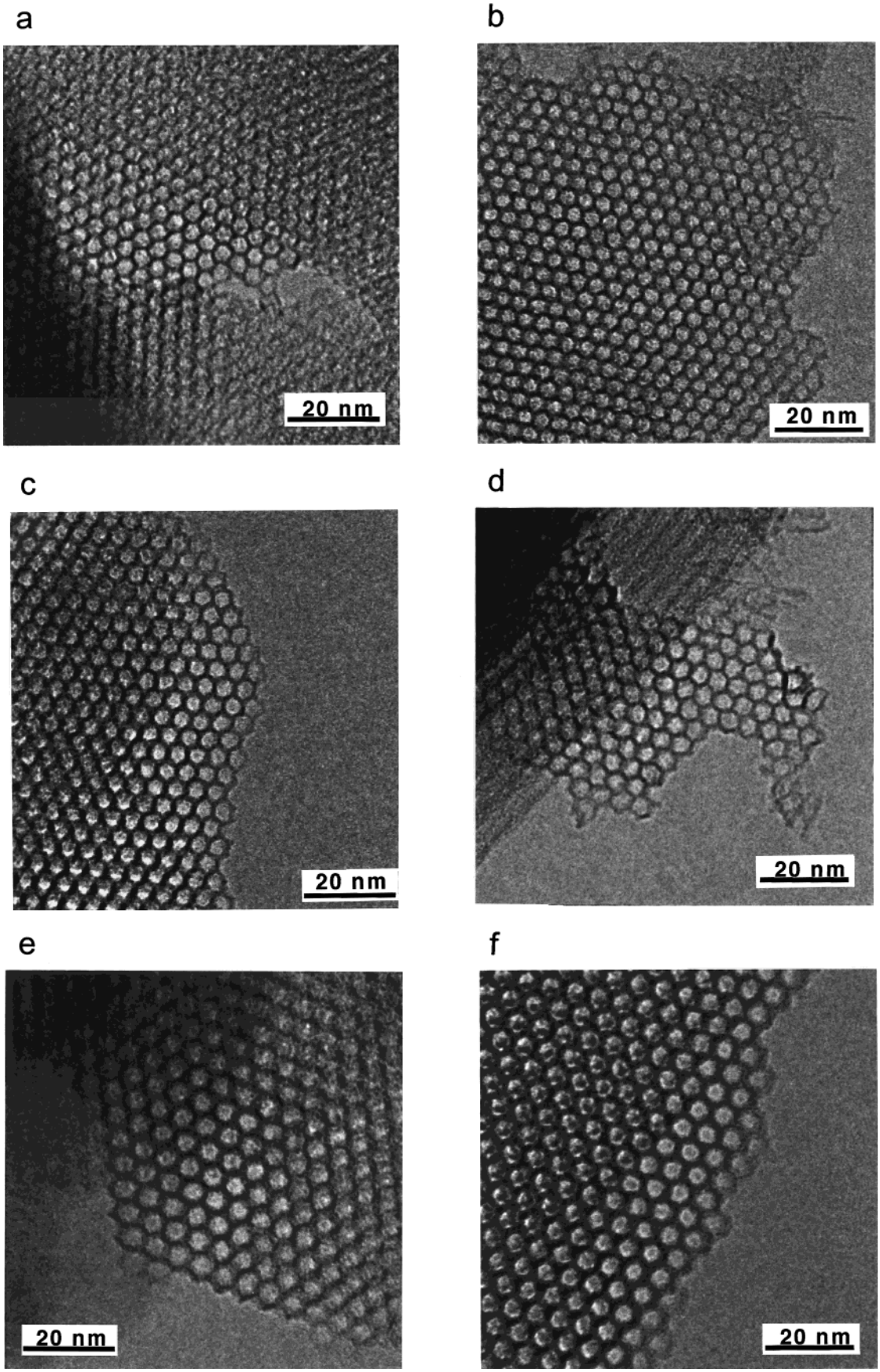

Figure 1. High-resolution transmission electron microscopy images for selected MCM-41 samples: (a) C14 EtOH/HCl washed; (b) C14 calcined; (c) C16 EtOH/HCl washed; (d) C16 calcined; (e) C22 EtOH/HCl washed; (f) C22 calcined.

3.2. High-Resolution Transmission Electron Microscopy. HRTEM images for selected calcined as well as EtOH/HCl washed samples are shown in Figure 1. The unit cell parameters and pore wall thicknesses derived from the HRTEM data are

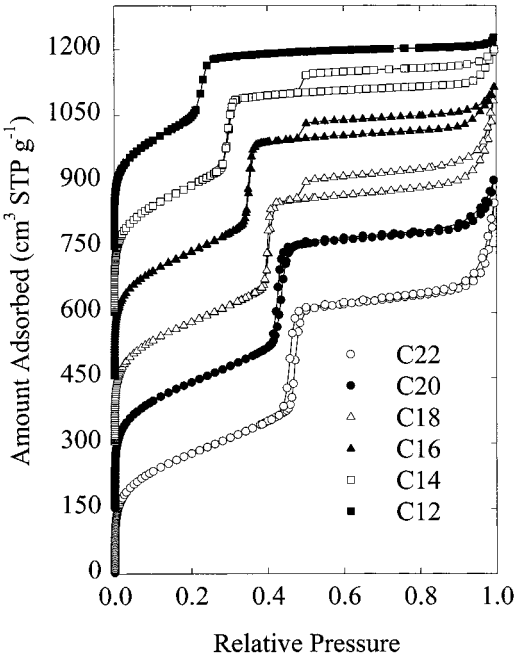

Figure 2. Nitrogen adsorption isotherms for the calcined MCM-41 silicas (amounts adsorbed for C20, C18, C16, C14, and C12 were incremented by 150, 300, 450, 600, and 750 cm^3 STP g^{-1}, respectively).

listed in Table 2. The obtained unit cell parameters were close to those evaluated using XRD, indicating a proper calibration of electron microscopy magnification. The pore wall thickness was usually found to be larger for uncalcined samples than for the calcined ones,[25] which is probably related to the shrinkage of the structure upon calcination. It can be seen in Figure 1 that the MCM-41 pores are approximately hexagonal rather than cylindrical. This is in accord with earlier findings,[23] but it is not yet fully clear if the hexagonal pore shape is a general feature of MCM-41 or just a feature of certain highly ordered samples. Materials of lower degree of structural ordering may exhibit larger deviations from the hexagonal pore shape. It is also interesting that the pore walls on the edges of particles were found to exhibit similar shape and thickness as those inside the particles. However, this feature requires further verification, since the samples were crushed before their TEM imaging. It should also be noted that in comparison to the uncalcined (for instance the EtOH/HCl washed) samples, the calcined ones appeared to have slightly lower degree of the pore structure ordering.

3.3. Nitrogen Adsorption. *Nitrogen Adsorption Isotherms.* Nitrogen adsorption isotherms for the calcined MCM-41 samples under study (Figure 2 and tabular data provided as Supporting Information) featured sharp capillary condensation steps. As the chain length of the surfactants used for the synthesis was increased, the position of the capillary condensation step gradually shifted from the relative pressure of about 0.22 to about 0.47. This shift indicated a systematic pore size increase, which can also be expected on the basis of the systematic changes in the unit cell parameter for the MCM-41 samples. The pore size distributions for the materials under study are shown in Figure 3 and exhibited sharp peaks with maxima uniformly covering the pore size range from 3.1 to 4.7 nm. The pore size increase was about 0.3 nm per each additional $-(CH_2)_2-$ unit. This demonstrates that the synthesis procedure used in the current study is suitable for fine-tuning of pore dimensions by judiciously choosing a surfactant with a proper chain length. As can be seen in Table 3, the pore sizes calculated using the BJH method with KJS calibration [17] were in excellent

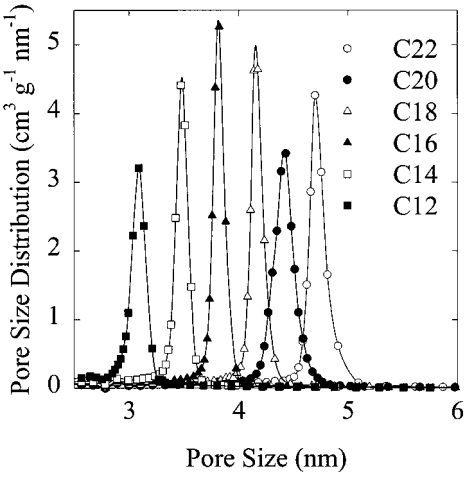

Figure 3. Mesopore size distributions for the calcined MCM-41 silicas.

agreement (differences not exceeding 0.1 nm) with pore sizes evaluated on the basis of the geometrical method (eq 1). This provides a confirmation of the great usefulness of the corrected Kelvin equation in the pore size analysis.

Pore Wall Thickness. As the pore size increased, pore wall thicknesses evaluated using the geometrical method were found to increase from 0.87 to 1.07 nm (Table 2). These pore wall thicknesses were somewhat smaller from those evaluated from the HRTEM, being 0.2−0.8 nm lower than the latter, which can be attributed to inherent features of these two evaluation methods. From its very nature, the geometrical approach allows one to evaluate an average pore wall thickness for the whole MCM-41 structure. In contrast, HRTEM probes the pore wall thickness perpendicular to the electron beam. Consequently, HRTEM pore wall thickness tends to be larger than the actual wall thickness when the main pore axis is not fully coincidental with the direction of the electron beam or the pores are bent to some extent.[25,28] Moreover, any kind of pore wall thickness fluctuation along the channels is likely to increase the HRTEM estimate of the pore wall thickness from its average value. The observed differences between the pore wall thickness estimates from combined XRD/nitrogen adsorption analysis and TEM were similar to those observed[25] between estimates from simulation of XRD patterns and TEM for calcined FSM-16, which is structurally similar to MCM-41. It should be noted that many common sources of differences between the HRTEM pore wall thickness and the actual pore wall thickness, such as improper calibration of electron microscopy magnification and lack of simulation of TEM images were eliminated in the current work.

Specific Surface Area and Pore Volume. Nitrogen adsorption isotherms for the MCM-41 samples under study indicated the presence of certain amounts of secondary mesopores in porous structures of these materials. C12 had very low secondary mesoporosity and almost no hysteresis in the high-pressure range. It should be noted that the secondary mesopore volume can be estimated as a difference between the primary mesopore volume and the total pore volume. In contrast to C12 MCM-41, the other samples exhibited pronounced hysteresis loops at higher pressures. The corresponding secondary mesopore volumes were also considerable (0.17−0.36 cm^3/g). The MCM-41 materials had very similar BET specific surface areas of about 1000 m^2/g. The primary mesopore volume, the total pore volume, and external surface area tend to decrease as the pore size decreased, but some small exceptions from this pattern of behavior were observed (see Table 3).

TABLE 3: Structural Properties of the Calcined MCM-41 Samples

sample	BET specific surface area (m^2/g)	total pore volume (cm^3/g)	primary mesopore volume (cm^3/g)	external surface area (m^2/g)	pore diameter (eq 1) (nm)	KJS pore diameter (nm)
C22	1000	1.23	0.87	140	4.80	4.70
C20	1040	1.12	0.88	110	4.51	4.41
C18	1010	1.14	0.79	140	4.14	4.16
C16	1050	1.00	0.81	80	3.87	3.80
C14	1050	0.92	0.75	50	3.51	3.47
C12	1030	0.73	0.68	20	3.16	3.09

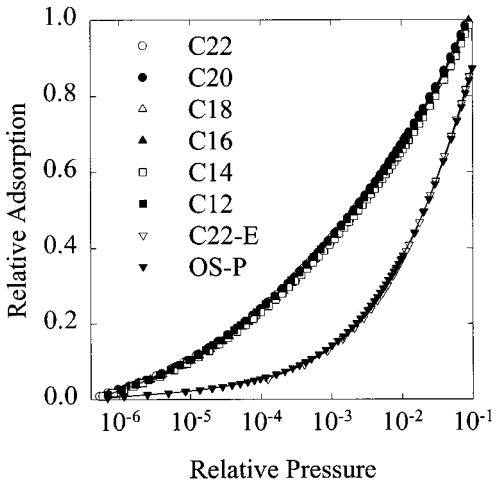

Figure 4. Relative adsorption curves for the calcined MCM-41 silicas, uncalcined ethanol-washed C22-E MCM-41, and an MCM-41 silica chemically modified with the polymeric octylsilyl phase.[42]

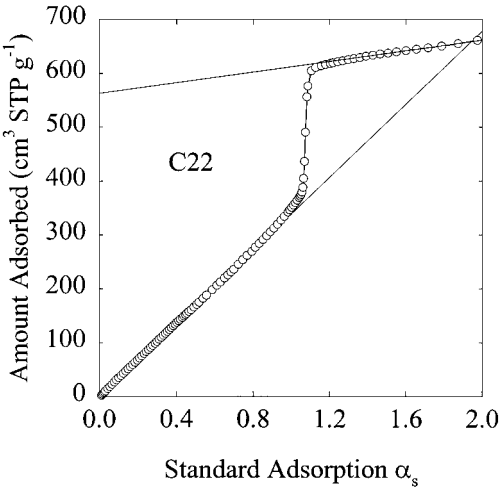

Figure 5. α_s-Plot for the calcined C22 MCM-41.

Low-Pressure Adsorption. As can be seen in Figure 4, low-pressure adsorption data were found to be highly similar for all the MCM-41 samples under study. To compare the adsorption behavior of these materials with that of the reference macroporous silicas, α_s plots were obtained and exhibited the same general behavior (see for instance the α_s plot for C22 MCM-41 shown in Figure 5). The initial parts of these plots were remarkably linear starting from their origin, which provided a convincing evidence of the absence of any detectable amounts of micropores. At higher pressures (or equivalently, higher α_s values), these plots exhibited sharp upward deviations caused by capillary condensation in primary mesopores. In the pressure range where the primary mesopores were essentially filled with the condensed adsorbate, the plots leveled off, but at pressures close to the saturation vapor pressure (α_s above about 2), some departures from linearity due to capillary condensation in secondary mesopores were observed.

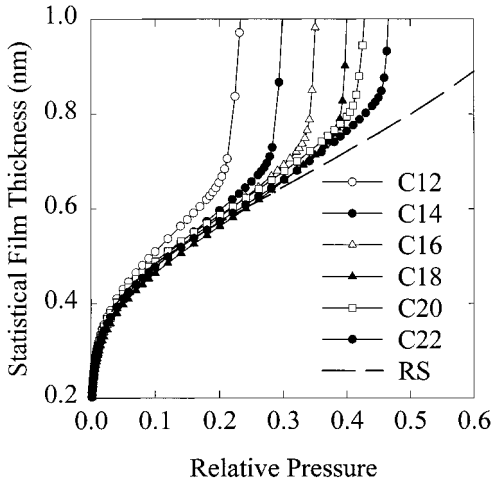

Figure 6. Statistical film thickness curves derived from nitrogen adsorption isotherms for the calcined MCM-41 silicas and a reference macroporous silica (RS).[17]

Statistical Film Thickness Curves. Since the MCM-41 samples under study exhibited a remarkable degree of the structural ordering, it was interesting to calculate the statistical film thickness curves (*t* curves) from nitrogen adsorption data and compare them with the *t* curve recently derived for porous silicas.[17] As can be seen in Figure 6, the *t* curves for the MCM-41 materials followed the *t* curve for the reference macroporous silica gel but exhibited gradually increasing deviations from the latter as the capillary condensation pressure was approached at which abrupt departures from the reference *t* curve were observed. In general, these departures from the reference *t* curve before the onset of capillary condensation were of quite small magnitude and were relatively less pronounced for the samples with larger pore sizes.[18] So, it can be concluded that the *t* curve derived for the macroporous silica can be used to adequately approximate the statistical film thickness in pores of MCM-41. It should be noted that the reference *t* curve shown was derived under the assumption of circular pore geometry of MCM-41 pores. Likewise, the *t* curves for the MCM-41 materials under study were calculated using the same assumption. In the case of the hexagonal pore geometry, these estimates of the statistical film thickness are about 5% lower. Thus, the *t* curves shown in Figure 6 can be regarded as effective statistical film thickness curves for hypothetical circular pore geometry, whereas the actual film thickness is about 5% lower.

Confirmation of the Corrected Kelvin Equation Derived Using the KJS Approach. The adsorption data for the high-quality MCM-41 samples were also used to examine the validity of the corrected Kelvin equation derived using the KJS approach (eq 2).[17] It can be seen in Figure 7 that the capillary condensation pressures closely followed the predictions of this equation, which is remarkable since its derivation was based on the application of MCM-41 samples of much lower degree of structural ordering than that of the materials described in this work. This indicates that even MCM-41 samples of moderate degree of structural

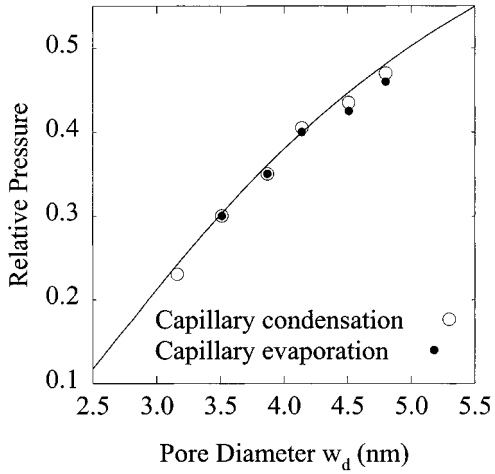

Figure 7. Relation between the pore diameter and the capillary condensation/evaporation pressure for the calcined MCM-41 silicas. Solid line calculated according to eq 2.

ordering can serve as model materials for calibration of many methods of adsorption data analysis. However, in some cases, there might be marked distinctions between the adsorption behavior of highly ordered and less-ordered MCM-41. For instance, C22 MCM-41 exhibited a very narrow hysteresis loop with approximately parallel adsorption and desorption branches. In the case of nitrogen at 77 K, hysteresis loops with parallel branches have been reported so far for MCM-41 samples with pore sizes above 5.5 nm,[17,38] whereas samples with lower pore sizes (between about 4 to 5.5 nm) were shown to exhibit triangular hysteresis loops with steep desorption branches.[17,18,42−45] It has already been reported that the shape and width of the hysteresis loops on adsorption isotherms for MCM-41 depends on the quality of the samples. In general, the relative pressure at which capillary condensation takes place was found to be a function of the pore size, whereas the steepness of the capillary condensation step reflected the quality of materials.[17] The relative pressure of capillary evaporation was considerably affected by the structural ordering of MCM-41 samples and the steepness of capillary evaporation steps was often related to the proximity of the lower limit of adsorption−desorption reversibility[17,35] rather than to the structural ordering of materials.[17] These findings were explained as a result of single-pore blocking effects related to the presence of constrictions in the channels of MCM-41 samples.[17] These effects were suggested to affect primarily the position and shape of desorption branches of hysteresis loops and to have a small influence, if any, on the adsorption branches of the isotherms.[17] The adsorption data for C22 MCM-41 confirmed this hypothesis, as the desorption behavior of this highly ordered sample was indeed found to be markedly different from those of the materials with a lower degree of structural ordering and yet the position of the adsorption branch of the isotherm was accurately predicted on the basis of the approach calibrated on MCM-41 with lower degree of structural ordering (see Figure 7). Because of the presence of very narrow hysteresis loop with parallel branches on its adsorption isotherm, one can expect that C22 MCM-41 exhibited a remarkable uniformity of the pore diameter along its mesoporous channels. One can expect that studies of such highly ordered model materials may provide much insight into adsorption−desorption behavior of ideal uniform pores, especially as far as desorption and hysteresis in such pores are concerned.

Nitrogen Adsorption Properties of Uncalcined Ethanol-Washed MCM-41 Samples. As was discussed above, most of the samples under study exhibited pronounced high-pressure hysteresis loops on their nitrogen adsorption isotherms, and their external surface areas as well as secondary mesopore volumes were significant. It would be interesting to verify whether the secondary mesopores formed during the hydrothermal synthesis or later as a result of the partial collapse upon calcination. The latter would indicate that the as-synthesized materials contain some impurities, presumably layered structures.[1,23,24] Thus, nitrogen adsorption isotherms were acquired for uncalcined ethanol-washed samples. As can be seen in Figure 8, these materials exhibited essentially the same shape of hysteresis loops in the high pressure range as the corresponding calcined samples. The secondary mesopore volume of the uncalcined materials was also related to that of the calcined samples, although it was somewhat lower (see Table 4), largely because the presence of surfactant in the uncalcined samples. This indicated that secondary mesoporosity of the calcined samples is determined primarily during the synthesis rather than during calcination, and thus is likely to be related to the structure of the MCM-41 particles. The presence of surfactant in the structure of uncalcined ethanol-washed samples was clearly demonstrated using TGA. The samples exhibited significant weight losses (see Table 4), mainly in the range from 430 to 773 K, which can be attributed mostly to the loss of surfactant and to a smaller extent, the release of water formed as a result of silanol condensation in the structure.[22] Except for C12-E, the primary mesopores of the uncalcined ethanol-washed materials were accessible only to a very small extent to nitrogen molecules (see primary mesopore volumes listed in Table 4). C12-E had some accessible porosity, but the equilibration of nitrogen in the pores during the adsorption run was very slow, which indicated diffusion problems in the structure. Therefore, the C12-E sample does not appear to be useful as an adsorbent. However, it is noteworthy that C12-E is a truly microporous ordered surfactant−silica composite with the maximum of the pore size distribution centered at 1.8 nm. The pore size was evaluated using a special procedure calibrated for hydrophobic silica-based materials and thus is reliable,[21] in contrast to commonly

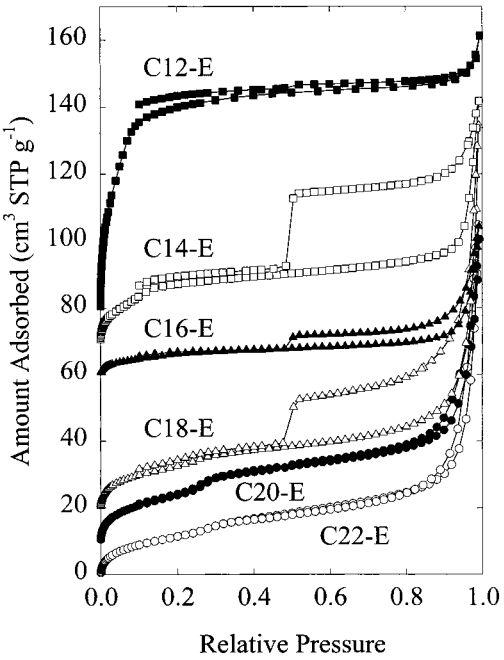

Figure 8. Nitrogen adsorption isotherms for uncalcined ethanol-washed MCM-41 silicas (amounts adsorbed for C20-E, C18-E, C16-E, C14-E, and C12-E were incremented by 10, 20, 60, 70, and 80 cm^3 STP g^{-1}, respectively).

TABLE 4: Specific Surface Areas and Pore Volumes of the As-Synthesized Ethanol-Washed MCM-41 Samples

sample	BET specific surface area ($m^2\ g^{-1}$)	BET relative pressure range	total pore volume ($cm^3\ g^{-1}$)	primary mesopore volume ($cm^3\ g^{-1}$)	external surface area ($m^2\ g^{-1}$)	TGA residue at 1270 K (%)
C22-E	44	0.04−0.2	0.16	0.01	28	57
C20-E	53	0.04−0.2	0.14	0.02	25	58
C18-E	47	0.04−0.2	0.18	0.01	25	58
C16-E	21	0.04−0.08	0.07	0.01	8	58
C14-E	63	0.04−0.08	0.11	0.02	16	61
C12-E	240	0.02−0.05	0.12	0.10	7	65

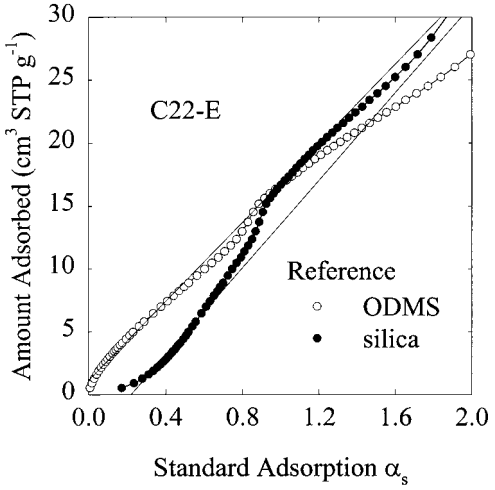

Figure 9. α_s-Plots for the uncalcined ethanol-washed C22-E MCM-41, calculated using reference adsorption isotherms for a macroporous silica (denoted as silica)[16,36] and for an octyldimethylsilyl-modified macroporous silica (denoted as ODMS).[21]

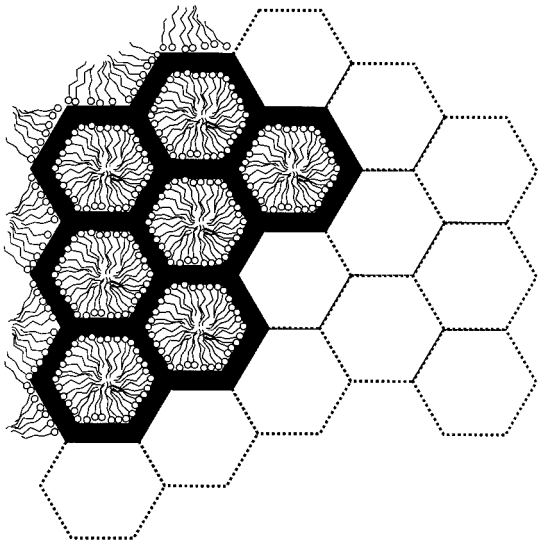

Figure 10. Schematic diagram of an as-synthesized MCM-41 particle. Note that the number of hexagons in the structure of actual particles is much larger, as can be seen in Figure 1.

employed procedures based on the noncorrected Kelvin equation, which lead to the pore size underestimation by about 1 nm,[17] thus indicating microporous character for some essentially mesoporous materials.

Low-Pressure Adsorption Properties of Uncalcined Ethanol-Washed MCM-41. Low-pressure nitrogen adsorption data for the uncalcined ethanol-washed samples revealed a very interesting feature of these materials. All of them exhibited relatively hydrophobic surfaces and their low-pressure adsorption properties resembled those of polymeric octylsilyl-modified silicas[42] (as seen in Figure 4 for C22-E MCM-41), rather than those of unmodified silicas, such as calcined MCM-41. The hydrophobic character of the surface of uncalcined ethanol-washed materials was also obvious from the comparative plot analysis. As can be seen in Figure 9, the application of silica as a reference adsorbent resulted in a highly nonlinear shape of the initial part of the α_s plot, which was bent downward indicating weak interactions of the C22-E surface with nitrogen molecules.[21,42] When an octyldimethylsilyl-modified silica (ODMS) was used as a reference, the initial part of the plot was much more linear but this time, it was bent upward, which indicated that surfaces covered with dense layers of ODMS ligands (such as those of the reference adsorbent used) interact more weakly with nitrogen than the surface of C22-E. Other uncalcined ethanol-washed samples exhibited similar surface properties, quite independently from the accessibility of primary mesopores of these materials. Thus, it can be concluded that external surfaces of the uncalcined ethanol-washed MCM-41 samples were hydrophobic.

The possible reason for the surface hydrophobicity is immediately apparent. It was convincingly demonstrated[46] that MCM-41 is usually formed via a multistep mechanism involving formation of ion pairs between surfactant ions and silicate oligomers. These ion pairs then self-assemble into the hexagonal structure, which is stabilized by the subsequent condensation of the silicate framework. Thus, one can expect that the outer part of the MCM-41 particles consists of silicates, which are not only covalently attached to the silicate framework but also carry electrostatically bonded surfactant molecules. Obviously, ion pairs can attach themselves to the surface of the already-formed particles differently, that is, the surfactant tail may interact with the tails of other surfactant molecules, which are electrostatically bonded to the silicate framework, whereas the silicate part may be at the exterior of the particle. However, this type of interaction of ion pairs with the already formed MCM-41 structure is much weaker, and such ion pairs may easily desorb from the particle's surface to the mother liquor or can readily be removed after washing. Thus, it is proposed that the external surface of particles of uncalcined surfactant-containing MCM-41 is covered to a significant extent with surfactant molecules electrostatically bonded to the silicate framework, and therefore is very similar to the internal surface of the these materials (see Figure 10). As a consequence, it is expected that the silicate walls on the exterior of the particles may be very similar to those in the interior of the particles. It should be noted that the bonding of the surfactant molecules to the external surface of MCM-41 particles is strong enough to withstand extensive ethanol washing, which is even capable of removing some weakly interacting species from the MCM-41 channels, or at least from the external part of these channels. This can be inferred from the fact that a certain volume of the primary mesopores was accessible to nitrogen molecules in the uncalcined ethanol-washed samples. It is also interesting that the properties of the external surface with respect to nitrogen molecules resemble closely the properties of surfaces of a polymeric alkylsilyl bonded phase. This may reflect the following structural similarity of these surfaces. Both of them feature highly hydrophobic moieties, such as long alkyl chains.

At the same time, in both cases, the coverage of these chains is not sufficient to screen the whole surface, and the more strongly interacting sites on the surface are still accessible to a small extent to nitrogen molecules.

Structure of the External Surface of MCM-41 Particles. HRTEM data lend support to the conclusion that the walls on the exterior of the particles are usually similar in terms of thickness and shape to those in the interior of the particles. This can be inferred from the TEM images reported before (see for instance refs 16, 39, and 47−51) and those presented in the current study (Figure 1). These images showed that the structure is composed of hexagons, although usually the resolution of the images reported before was not sufficient to determine the exact pore shape. The hexagons on the external surface typically have two sides exposed to the surrounding but three sides or one side exposed are also common, whereas hexagons with four external sides are rarely seen (see for instance Figure 1; schematic of different arrangements of hexagons on the external surface is shown in Figure 10). In addition, the HRTEM images presented in the current study allow one to draw a conclusion that the pores are hexagonal, rather than circular, and the pore walls on the exterior of the particles are similar to those in the interior of the particles. The latter conclusion requires further verification, since the samples were crushed before TEM imaging and thus it is not clear if the observed particle edges are those of the actual particles or those resulting from the crushing procedure. Moreover, it needs to be kept in mind that the aforementioned conclusion about the properties of the external surface of particles is not fully general. For instance, the exterior of particles of MCM-41, which underwent an extensive high-temperature hydrothermal treatment, showed signs of an appreciable structural degradation, which manifested itself in a nonhexagonal shape of the outermost layer of pores.[48]

Figure 10 provides a diagram that presents the most important of the above findings, illustrating the different local arrangements of hexagons on the external surface, and the fact that surfactant molecules are attached to the external surface of uncalcined surfactant-containing samples, as determined using low-pressure nitrogen adsorption. It should be noted that the formation of the hexagonal pore walls was already explained in terms of maintaining the constant pore wall thickness and thereby maximizing the surfactant−silicate interactions.[29,30] It was argued that the silicates at the interface have their charges compensated by the charges of surfactant ions and consequently do not repel each other to such an extent as free silicate anions and thus can readily condense with one another. At the same time, the electrostatic repulsion hinders silicate polymerization normal to the silicate−surfactant interface, thereby allowing to maintain the constant pore wall thickness.[23,29,30] It is also interesting to note here that the schematic representation of MCM-41 shown here (Figure 10) is similar to that suggested by Cheng et al.,[52] but the latter reflected only the short- and long-range arrangement of the surfactant micelles in the MCM-41 structure and did not show details of the pore wall structure.

The presence of surfactant molecules on the external surface of particles of uncalcined ethanol-washed samples was found to be a common feature of the MCM-41 samples under study. It is yet to be verified if it is a general property of templated mesoporous materials, but since they are commonly formed via self-assembly of surfactant−silicate ion pairs,[46] the electrostatic bonding of surfactant to the external surface is expected to be quite common. This in turn allows us to understand better why the as-prepared silicate−surfactant composites can so readily extend the size of their ordered domains, both at early stages of the synthesis[52−55] and upon aging,[9] and can undergo various phase transitions.[4,6,8]

Conclusions

The current study showed that the applied synthesis procedure allows for tailoring of the MCM-41 pore size and is suitable for preparation of high-quality materials. It was shown that the pore wall thickness properly estimated on the basis of adsorption/XRD data is in acceptable agreement with the results of HRTEM. The latter technique indicates somewhat larger pore wall thickness, which can be attributed, at least in part, to the very nature of the compared evaluation procedures. Both of these approaches consistently show that the pore wall thickness for the samples under study tends to increase as the pore size increases. In calculations of the pore wall thickness on the basis of adsorption/XRD data, it needs to be kept in mind that the pores of MCM-41 are likely to be hexagonal rather than circular, although it is not fully clear if this conclusion is general or just extends over certain MCM-41 silicas.

As seen from HRTEM data, the pore walls on the exterior of the MCM-41 particles are similar in shape and thickness to those in the interior of the particles, but this conclusion requires further verification, since the samples studied were crushed before the TEM measurements. Low-pressure nitrogen adsorption provided strong evidence that the external surface of uncalcined surfactant-containing MCM-41 particles is covered by a relatively dense layer of strongly bonded surfactant molecules. The aforementioned structural features of the external surface of particles may be important in processes of particle's growth. Moreover, the similarity of the pore wall structure throughout the whole particle may be important in phase transformations of surfactant−silicate composite materials.

Acknowledgment. The donors of the Petroleum Research Fund administrated by the American Chemical Society are gratefully acknowledged for a partial support of this research.

Supporting Information Available: Nitrogen adsorption−desorption isotherms measured at 77 K for the calcined MCM-41 samples under study are provided in the tabular form. This material is available free of charge via the Internet at http://pubs.acs.org.

References and Notes

(1) Beck, J. S.; Vartuli, J. C.; Roth, W. J.; Leonowicz, M. E.; Kresge, C. T.; Schmitt, K. D.; Chu, C. T−W.; Olson, D. H.; Sheppard, E. W.; McCullen, S. B.; Higgins, J. B.; Schlenker, J. L. *J. Am. Chem. Soc.* **1992**, *114*, 10834.

(2) Yanagisawa, T.; Shimizu, T.; Kuroda, K.; Kato, C. *Bull. Chem. Soc. Jpn.* **1990**, *63*, 988.

(3) Raman, N. K.; Anderson, M. T.; Brinker, C. J. *Chem. Mater.* **1996**, *8*, 1682.

(4) Sayari, A. *Stud. Surf. Sci. Catal.* **1996**, *102*, 1.

(5) Corma, A. *Chem. Rev.* **1997**, *97*, 2373.

(6) Stucky, G. D.; Huo, Q.; Firouzi, A.; Chmelka, B. F.; Schacht, S.; Voigt-Martin, I. G.; Schuth, F. *Stud. Surf. Sci. Catal.* **1997**, *105*, 3.

(7) Ying, J. Y.; Mehnert, C. P.; Wong, M. S. *Angew. Chem., Int. Ed. Engl.* **1999**, *38*, 56.

(8) Ciesla, U.; Schuth, F. *Microporous Mesoporous Mater.* **1999**, *27*, 131.

(9) Kruk, M.; Jaroniec, M.; Sayari, A. *J. Phys. Chem. B* **1999**, *103*, 4590.

(10) Sayari, A.; Liu, P. *Microporous Mater.* **1997**, *12*, 149.

(11) Sayari, A. *Chem. Mater.* **1996**, *8*, 1840.

(12) Kruk, M.; Jaroniec, M.; Sayari, A. *Chem. Mater.* **1999**, *11*, 492.

(13) Chen, C.-Y.; Xiao, S.-Q.; Davis, M. E. *Microporous Mater.* **1995**, *4*, 1.

(14) Dabadie, T.; Ayral, A.; Guizard, C.; Cot, L.; Lacan, P. *J. Mater. Chem.* **1996**, *6*, 1789.

(15) Kruk, M.; Jaroniec, M.; Sayari, A. *J. Phys. Chem. B* **1997**, *101*, 583.
(16) Kruk, M.; Jaroniec, M.; Ryoo, R.; Kim, J. M. *Microporous Mater.* **1997**, *12*, 93.
(17) Kruk, M.; Jaroniec, M.; Sayari, A. *Langmuir* **1997**, *13*, 6267.
(18) Kruk, M.; Jaroniec, M.; Kim, J. M.; Ryoo, R. *Langmuir* **1999**, *15*, 5279.
(19) Barrett, E. P.; Joyner, L. G.; Halenda, P. P. *J. Am. Chem. Soc.* **1951**, *73*, 373.
(20) Gregg, S. J.; Sing, K. S. W. *Adsorption, Surface Area and Porosity*; Academic Press: London, 1982.
(21) Kruk, M.; Antochshuk, V.; Jaroniec, M.; Sayari, A. *J. Phys. Chem. B* **1999**, *103*, 10670.
(22) Chen, C.-Y.; Li, H.-X.; Davis, M. E. *Microporous Mater*. **1993**, *2*, 17.
(23) Alfredsson, V.; Keung, M.; Monnier, A.; Stucky, G. D.; Unger, K. K.; Schuth, F. *J. Chem. Soc., Chem. Commun.* **1994**, 921.
(24) Chenite, A.; Le Page, Y.; Sayari, A. *Chem. Mater.* **1995**, *7*, 1015.
(25) Inagaki, S.; Sakamoto, Y.; Fukushima, Y.; Terasaki, O. *Chem. Mater.* **1996**, *8*, 2089.
(26) Alfredsson, V.; Anderson, M. W. *Chem. Mater.* **1996**, *8*, 1141.
(27) Schacht, S.; Janicke, M.; Schuth, F. *Microporous Mesoporous Mater.* **1998**, *22*, 485.
(28) Sakamoto, Y.; Inagaki, S.; Ohsuna, T.; Ohnishi, N.; Fukushima, Y.; Nozue, Y.; Terasaki, O. *Microporous Mesoporous Mater.* **1998**, *21*, 589.
(29) Monnier, A.; Schuth, F.; Huo, Q.; Kumar, D.; Margolese, D.; Maxwell, R. S.; Stucky, G. D.; Krishnamurty, M.; Petroff, P.; Firouzi, A.; Janicke, M.; Chmelka, B. F. *Science* **1993**, *261*, 1299.
(30) Stucky, G. D.; Monnier, A.; Schuth, F.; Huo, Q.; Margolese, D.; Kumar, D.; Krishnamurty, M.; Petroff, P.; Firouzi, A.; Janicke, M.; Chmelka, B. F. *Mol. Cryst. Liq. Cryst.* **1994**, *240*, 187.
(31) Feuston, B. P.; Higgins, J. B. *J. Phys. Chem.* **1994**, *98*, 4459.
(32) Ryoo, R.; Kim, J. M. *J. Chem. Soc., Chem. Commun.* **1995**, 711.
(33) Ryoo, R.; Jun, S. *J. Phys. Chem. B* **1997**, *101*, 317.
(34) Ryoo, R.; Ko, C. H.; Park, I.-S. *Chem. Commun.* **1999**, 1413.
(35) Sing, K. S. W.; Everett, D. H.; Haul, R. A. W.; Moscou, L.; Pierotti, R. A.; Rouquerol, J.; Siemieniewska, T. *Pure Appl. Chem.* **1985**, *57*, 603.
(36) Jaroniec, M.; Kruk, M.; Olivier, J. P. *Langmuir* **1999**, *15*, 5410.
(37) Huo, Q.; Margolese, D. I.; Ciesla, U.; Demuth, G. D.; Feng, P.; Gier, T. E.; Sieger, P.; Firouzi, A.; Chmelka, B. F.; Shüth, F.; Stucky, G. D. *Chem. Mater.* **1994**, *6*, 1176.
(38) Huo, Q.; Margolese, D. I.; Stucky, G. D. *Chem. Mater.* **1996**, *8*, 1147.
(39) Namba, S.; Mochizuki, A.; Kito, M. *Stud. Surf. Sci. Catal.* **1998**, *117*, 257.
(40) Khushalani, D.; Kuperman, A.; Coombs, N.; Ozin, G. A. *Chem. Mater.* **1996**, *8*, 2188.
(41) Chen, F.; Huang, L.; Li, Q. *Chem. Mater.* **1997**, *9*, 2685.
(42) Jaroniec, C. P.; Kruk, M.; Jaroniec, M.; Sayari, A. *J. Phys. Chem. B* **1999**, *102*, 5503.
(43) Llewellyn, P. L.; Grillet, Y.; Schuth, F.; Reichert, H.; Unger, K. K. *Microporous Mater.* **1994**, *3*, 345.
(44) Schmidt, R.; Stocker, M.; Hansen, E.; Akporiaye, D.; Ellestad, O. H. *Microporous Mater.* **1995**, *3*, 443.
(45) Chen, L.; Horiuchi, T.; Mori, T.; Maeda, K. *J. Phys. Chem. B* **1999**, *103*, 1216.
(46) Firouzi, A.; Kumar, D.; Bull, L. M.; Besier, T.; Sieger, P.; Huo, Q.; Walker, S. A.; Zasadzinski, J. A.; Glinka, C.; Nicol, J.; Margolese, D.; Stucky, G. D.; Chmelka, B. F. *Science* **1995**, *267*, 1138.
(47) Luan, Z.; Cheng, C.-F.; Zhou, W.; Klinowski, J. *J. Phys. Chem. B* **1995**, *99*, 1018.
(48) Cheng, C.-F.; Zhou, W.; Park, D. H.; Klinowski, J.; Hargreaves, M.; Gladden, L. F. *J. Chem. Soc., Faraday Trans.* **1997**, *93*, 359.
(49) Namba, S.; Mochizuki, A. *Res. Chem. Intermed.* **1998**, *24*, 561.
(50) Malakutla, R. S.; Asakura, K.; Namba, S.; Iwasawa, Y. *Chem. Commun.* **1998**, 1425.
(51) Miyata, H.; Kuroda, K. *Adv. Mater.* **1999**, *11*, 857.
(52) Cheng, C.-F.; He, H.; Zhou, W.; Klinowski, J. *Chem. Phys. Lett.* **1995**, *244*, 117.
(53) Regev, O. *Langmuir* **1996**, *12*, 4940.
(54) Zhang, J.; Luz, Z.; Goldfarb, D. *J. Phys. Chem. B* **1997**, *101*, 7087.
(55) Galarneau, A.; Di Renzo, F.; Fajula, F.; Mollo, L.; Fubini, B.; Ottaviani, M. F. *J. Colloid Interface Sci.* **1998**, *201*, 105.